Research Article

Vol. 25, No. 17 | 21 Aug 2017 | OPTICS EXPRESS 20530

Optics EXPRESS

Real and virtual propagation dynamics of angular accelerating white light beams

CHRISTIAN VETTER,[1] ANGELA DUDLEY,[2,3] ALEXANDER SZAMEIT,[1,4] AND ANDREW FORBES[3,*]

[1]*Institute of Applied Physics, Abbe Center of Photonics, Friedrich-Schiller-Universität Jena, 07745 Jena, Germany*
[2]*CSIR National Laser Centre, PO Box 395, Pretoria 0001, South Africa*
[3]*School of Physics, University of the Witwatersrand, Johannesburg 2050, South Africa*
[4]*Institute for Physics, University of Rostock, 18059 Rostock, Germany*
[*]*andrew.forbes@wits.ac.za*

Abstract: Accelerating waves have received significant attention of late, first in the optical domain and later in the form of electron matter waves, and have found numerous applications in non-linear optics, material processing, microscopy, particle manipulation and laser plasma interactions. Here we create angular accelerating light beams with a potentially unlimited acceleration rate. By employing wavelength independent digital holograms for the creation and propagation of white light beams, we are able to study the resulting propagation in real and virtual space. We find that dephasing occurs for real propagation and that this can be compensated for in a virtual propagation scheme when single plane dynamics are important. Our work offers new insights into the propagation dynamics of such beams and provides a versatile tool for further investigations into propagating structured light fields.

References and links

1. H. Rubinsztein-Dunlop, A. Forbes, M. Berry, M. Dennis, D. L. Andrews, M. Mansuripur, C. Denz, C. Alpmann, P. Banzer, T. Bauer, E. Karimi, L. Marrucci, M. Padgett, M. Ritsch-Marte, N. M. Litchinitser, N. P. Bigelow, C. Rosales-Guzmán, A. Belmonte, J. P. Torres, T. W. Neely, M. Baker, R. Gordon, A. B. Stilgoe, J. Romero, A. G. White, R. Fickler, A. E. Willner, G. Xie, B. McMorran and A. M. Weiner, "Roadmap on structured light," J. Opt. **19**, 013001 (2017).
2. G. A. Siviloglou and D. N. Christodoulides, "Accelerating finite energy airy beams," J. Opt. **32**, 979–981 (2007).
3. G. A. Siviloglou, J. Broky, A. Dogariu, and D. N. Christodoulides, "Observation of accelerating airy beams," Phys. Rev. Lett. **99**, 213901 (2007).
4. M. A. Bandres, "Accelerating parabolic beams," Opt. Lett. **33**, 1678–1680 (2008).
5. C. Vetter, T. Eichelkraut, M. Ornigotti, and A. Szameit, "Generalized radially self-accelerating helicon beams," Phys. Rev. Lett. **113**, 183901 (2014).
6. C. Schulze, F. S. Roux, A. Dudley, R. Rop, M. Duparre, and A. Forbes, "Accelerated rotation with orbital angular momentum modes," Phys. Rev. A **91**, 043821 (2015).
7. J. Webster, C. Rosales-Guzmán, and A. Forbes, "Radially dependent angular acceleration of twisted light," Opt. Lett. **42**, 675–678 (2017).
8. J. Arlt and M. Padgett, "Generation of a beam with a dark focus surrounded by regions of higher intensity: the optical bottle beam," Opt. Lett. **25**, 191–193 (2000).
9. J. C. Gutíerrez-Vega, M. Iturbe-Castillo, G. Ramírez, E. Tepichín, R. Rodríguez-Dagnino, S. Chávez-Cerda, and G. New, "Experimental demonstration of optical mathieu beams," Opt. Commun. **195**, 35–40 (2001).
10. P. Zhang, Y. Hu, T. Li, D. Cannan, X. Yin, R. Morandotti, Z. Chen, and X. Zhang, "Nonparaxial mathieu and weber accelerating beams," Phys. Rev. Lett. **109**, 193901 (2012).
11. J. Y. Lu, Y. and J. F. Greenleaf, "Nondiffracting x-waves - exact-solutions to free-space scalar wave-equation and their finite aperture realizations," IEEE Transactions On Ultrasonics Ferroelectrics and Frequency Control **39**, 19–31 (1992).
12. Y. Lumer, Y. Liang, R. Schley, I. Kaminer, E. Greenfield, D. Song, X. Zhang, J. Xu, Z. Chen, and M. Segev, "Incoherent self-accelerating beams," Optica **2**, 886–892 (2015).
13. T. Eichelkraut, C. Vetter, A. Perez-Leija, and A. Szameit, "Coherent random walks in free space," Optica **1**, 268–271 (2014).
14. T. Vettenburg, H. I. C. Dalgarno, J. Nylk, C. Coll-Llado, D. E. K. Ferrier, T. Cizmar, F. J. Gunn-Moore, and K. Dholakia, "Light-sheet microscopy using an airy beam," Nat. Methods **11**, 541–544 (2014).

15. J. Baumgartl, M. Mazilu, and K. Dholakia, "Optically mediated particle clearing using airy wavepackets," Nat. Photon. **2**, 675–678 (2008).
16. N. K. Efremidis and D. N. Christodoulides, "Abruptly autofocusing waves," Opt. Lett. **35**, 4045–4047 (2010).
17. R. Steiger, S. Bernet, and M. Ritsch-Marte, "Slm-based off-axis fourier filtering in microscopy with white light illumination," Opt. Express **20**, 15377–15384 (2012).
18. C. Maurer, A. Jesacher, S. Bernet, and M. Ritsch-Marte, "What spatial light modulators can do for optical microscopy," Laser Photon. Rev. **5**, 81–101 (2011).
19. D. Grier and S. Lee, "Multi-color holographic optical traps," (2010). US Patent 7,759,020.
20. A. Mathis, L. Froehly, L. Furfaro, M. Jacquot, J. M. Dudley, and F. Courvoisier, "Direct machining of curved trenches in silicon with femtosecond accelerating beams," J. Eur. Opt. Soc, Rapid Publ. **8**, 13019 (2013).
21. P. Polynkin, M. Kolesik, J. V. Moloney, G. A. Siviloglou, and D. N. Christodoulides, "Curved plasma channel generation using ultraintense airy beams," Science **324**, 229–232 (2009).
22. R. Piestun, Y. Y. Schechner, and J. Shamir, "Propagation-invariant wave fields with finite energy," J. Opt. Soc. Am. A **17**, 294–303 (2000).
23. Y. Y. Schechner, R. Piestun, and S. Shamir, "Wave propagation with rotating intensity distributions," Phys. Rev. E **54**, R50–R53 (1996).
24. C. Paterson and R. Smith, "Helicon waves: Propagation-invariant waves in a rotating coordinate system," Opt. Commun. **124**, 131–140 (1996).
25. R. Vasilyeu, A. Dudley, N. Khilo, and A. Forbes, "Generating superpositions of higher-order bessel beams," Opt. Express **17**, 23389–23395 (2009).
26. R. Rop, I. A. Litvin, and A. Forbes, "Generation and propagation dynamics of obstructed and unobstructed rotating orbital angular momentum-carrying helicon beams," J. Opt. **14**, 035702 (2012).
27. C. Vetter, T. Eichelkraut, M. Ornigotti, and A. Szameit, "Optimization and control of two-component radially self-accelerating beams," Appl. Phys. Lett. **107**, 211104 (2015).
28. A. Forbes, A. Dudley, and M. McLaren, "Creation and detection of optical modes with spatial light modulators," Adv. Opt. Photonics **8**, 200–227 (2016).
29. J. L. Martinez, E. J. Fernandez, P. M. Prieto, and P. Artal, "Chromatic aberration control with liquid crystal spatial phase modulators," Opt. Express **25**, 9793–9801 (2017).
30. D.-M. Spangenberg, A. Dudley, P. H. Neethling, E. G. Rohwer, and A. Forbes, "White light wavefront control with a spatial light modulator," Opt. Express **22**, 13870–13879 (2014).
31. C. Schulze, D. Flamm, M. Duparre, and A. Forbes, "Beam-quality measurements using a spatial light modulator," Opt. Lett. **37**, 4687–4689 (2012).
32. J. A. Davis, I. Moreno, D. M. Cottrell, C. A. Berg, C. L. Freeman, A. Carmona, and W. Debenham, "Experimental implementation of a virtual optical beam propagator system based on a fresnel diffraction algorithm," Opt. Eng. **54**, 103101 (2015).
33. J. Durnin, J. J. Miceli, and J. H. Eberly, "Diffraction-free beams," Phys. Rev. Lett. **58**, 1499–1501 (1987).
34. J. Durnin, "Exact-solutions for nondiffracting beams 1 – the scalar theory," J. Opt. Soc. Am. A **4**, 651–654 (1987).
35. J. A. Davis, D. M. Cottrell, J. Campos, M. J. Yzuel, and I. Moreno, "Encoding amplitude information onto phase-only filters," Appl. Opt. **38**, 5004–5013 (1999).

1. Introduction

Over the last decade the demand for complex optical beam shapes has grown rapidly [1]. One manifestation of this demand is reflected in the enormous diversity of new self-accelerating beams with carrier fields such as Airy Beams [2,3], parabolic beams [4], radially self-accelerating beams [5], angular self-accelerating beams [6,7], bottle beams [8], Mathieu beams [9,10], X-waves [11], incoherent accelerating beams [12] as well as beams that resemble the propagation of coherent random walkers in free space [13]. With more and more of those fundamentally interesting phenomena finding their way into novel applications [14–16] it seems obvious, that many of them might benefit from a broadband or multiline spectral approach. This is especially true for optical microscopy [17,18], particle manipulation [19] and ultrafast laser applications [20,21]. Unfortunately most beam shaping techniques rely on phase-only devices such as spatial light modulators (SLMs) or diffractive optical elements that are inherently wavelength dependent and thus do not appear to be suited for white light applications.

Despite the wavelength dependence of such devices, here we create and propagate white light angular accelerating beams using a phase-only SLM. We summarise how it is possible to design wavelength independent holograms, such that each spectral component obtains the correct phase distribution with only minor amplitude perturbations. We find that in real propagation the spectral components dephase over distance. However, by deploying the holograms in the angular spectrum domain (the far field of the desired observation plane) we are able to implement a virtual propagation tool that allows us to investigate the propagation dynamics without the need for any moving parts. Intriguingly, we find that the virtual propagation in conjunction with the wavelength independent holographic implementation becomes fully non-dispersive. In other words, the spectral components of the beam behave as if the wave number k would be a wavelength independent constant. This allows for the accelerating dynamics to remain intact across a broad wavelength range when observing a single plane. Our work offers new insights into the propagation dynamics of such accelerating white light beams, and provides a versatile tool for further study of propagating structured white light fields in general.

2. Theory

In this section we provide a generalised description of angular accelerating waves and introduce the core toolbox for this study. That is to say, we explain how to create the aforementioned waves via complex amplitude modulation in a wavelength independent manner and we show how to digitally propagate them such that the propagation itself appears to be non-dispersive. While the tools for wavelength independent holography and virtual propagation do exist, here we bring them together into a single hologram to study white light propagation, and thus outline the core concepts in this section for the benefit of the reader.

2.1. Construction of angular accelerating waves

The fundamental concept of rotating, shape-invariant beams was outlined some time ago and serves as a guideline for defining [22] and realising [23] such field configurations. Here we restrict our attention to a recently introduced class of optical beams with helical trajectories and periodically varying rotation rates [6]. In the context of self-acceleration, one would regard that as a radial- and (at the same time) angular acceleration scheme. This is because a co-moving observer would experience not just a radial centrifugal force but on top of that a periodic acceleration and deceleration in the azimuthal direction. First however, let us discuss how beams with helical trajectories can be understood. A very common way, though not the most general one [5,22], are classical helicon beams [24–27]. They are based on the interference of two Bessel waves with different helical phase orders (m, ℓ) and propagation terms $(k_{z|1}, k_{z|2})$. In a circular cylindrical coordinate system this reads as follows

$$u(r, \varphi, z) = \mathcal{J}_m(k_{r|1}r)\, e^{im\varphi}e^{izk_{z|1}} + \mathcal{J}_\ell(k_{r|2}r)\, e^{i\ell\varphi}e^{izk_{z|2}}, \tag{1}$$

$$\begin{aligned}|u(r, \varphi, z)|^2 = &\left|\mathcal{J}_m(k_{r|1}r)\right|^2 + \left|\mathcal{J}_\ell(k_{r|2}r)\right|^2 \\ &+ 2\,\mathcal{J}_m(k_{r|1}r)\,\mathcal{J}_\ell(k_{r|2}r)\cos(\Delta_{m\ell}\varphi + \Delta k_z z).\end{aligned} \tag{2}$$

Here, $\mathcal{J}_m(k_r r)$ denotes the Bessel function of the first kind and order m with k_r being the radial component to the wave number that relates to the propagation constant via $k_r = \sqrt{k^2 - k_z^2}$. Moreover, for convenience, we defined $\Delta_{m\ell} = m - \ell$ and $\Delta k_z = k_{z|1} - k_{z|2}$. Equation (2) immediately shows the structure for a helical trajectory. It also indicates, that all iso-intensity curves obey $\Delta_{m\ell}\,\varphi + \Delta k_z z = \varphi_0$ with φ_0 being an arbitrary constant. From this, the rotation angle $\varphi(z)$, rotation rate $\omega(z)$ and angular acceleration $\alpha(z)$ can be derived.

$$\varphi(z) = \frac{\varphi_0 - \Delta k_z z}{\Delta_{m\ell}} \qquad \omega(z) = \frac{\mathrm{d}\varphi(z)}{\mathrm{d}z} = -\frac{\Delta k_z}{\Delta_{m\ell}} \qquad \alpha(z) = \frac{\mathrm{d}^2\varphi(z)}{\mathrm{d}z^2} = 0$$

As expected, since helicon beams do not exhibit a variable rotation rate, the angular acceleration drops to zero. To achieve non-vanishing acceleration, it is important to understand how the helical trajectory is formed. Due to the different propagation constants, the phase fronts of both input fields continuously dephase with respect to each other causing the helical phase fronts to interfere along a spiraling path. Hence one approach to create beams with a variable rotation rate is to use non-linear helical phase terms, as was done in Ref. [6] using a clever combination of linearly-phased Bessel waves, thus still satisfying the scalar Helmholtz equation. Let's assume a new input field $u(r, \varphi, z) \equiv g_m(r, \varphi, z, \eta)$ with

$$g_m(r, \varphi, z, \eta) = \mathcal{J}_m(k_r r) \left[\cos(\eta/2) \, e^{im\varphi} + \sin(\eta/2) \, e^{-im\varphi} \right] e^{ik_z z}. \tag{3}$$

This field is just a superposition of two Bessel waves but it exhibits a non-linear instead of the usual linear helical phase ramp. The new conditional variable η is a measure for this non-linearity. Values $\eta \approx 0$ infer a near-linear phase behavior while values $\eta \approx \pi/2$ result in an almost step-like function. Note, that by choosing values $\eta > \pi/2$ one flips the slope of the phase ramp which is equivalent to changing the sign of m; thus $g_{-m}(r, \varphi, z, \eta) = g_m(r, \varphi, z, \pi - \eta)$. By superimposing two of those fields (similarly as in the case of Eq. (1)) whereby we change the sign of $|m|$, we obtain

$$
\begin{aligned}
u(r, \varphi, z) = \; & \mathcal{J}_m\left(k_{r|1}r\right) \left[\cos(\eta/2) \, e^{im\varphi} + \sin(\eta/2) \, e^{-im\varphi} \right] e^{ik_{z|1}z} \\
& + \mathcal{J}_{-m}\left(k_{r|2}r\right) \left[\cos(\eta/2) \, e^{-im\varphi} + \sin(\eta/2) \, e^{im\varphi} \right] e^{ik_{z|2}z}.
\end{aligned}
\tag{4}
$$

Subsequently, we can calculate the resulting field's intensity $|u(r, \varphi, z)|^2$, and, like before, use it to obtain the rotation characteristics of the beam:

$$\varphi(z) = \frac{1}{2 \, |m|} \arctan \left[\frac{\cos(\eta) \sin(\Delta k_z z)}{\sin(\eta) + \cos(\Delta k_z z)} \right] \tag{5}$$

$$\omega(z) = \frac{\Delta k_z}{2 \, |m|} \frac{\cos(\eta)}{1 + \sin(\eta) \cos(\Delta k_z z)} \tag{6}$$

$$\alpha(z) = \frac{\Delta k_z^2}{4 \, |m|} \frac{\sin(2\eta) \sin(\Delta k_z z)}{[1 + \sin(\eta) \cos(\Delta k_z z)]^2} \tag{7}$$

Since the superposition involves two fields with non-canonical phase orders of opposite sign, the angular acceleration term is now non-vanishing. Moreover, notice that for $\eta \to \pi/2$, the angular acceleration $\alpha(z)$ diverges to infinity. This is a unique and potentially very useful characteristic which is difficult, if not impossible, to achieve with other acceleration schemes. This is because in the angular accelerating case the acceleration takes place in a bounded space - the azimuthal plane. Thus very large accelerations can be realised without the need for a large transverse space. Conversely, in transverse accelerating beams ever more transverse space is needed to observe higher accelerations, and this eventually causes the paraxial limit to be broken. Importantly, though, in the actual acceleration region there is a predicted spatial energy transfer in order to conserve angular momentum that is also dependent on η. As the field accelerates and decelerates during propagation, so energy is transferred in and out of the central region. This effect has been confirmed experimentally [6].

2.2. Wavelength independent complex amplitude modulation

When creating self-accelerating optical fields, simultaneous amplitude and phase manipulation on a single phase-only device is often required. It is possible, by complex amplitude modulation, to create any optical field in amplitude and phase on a phase-only SLM (see Ref. [28] and references therein for the various techniques). While controlling monochromatic fields is self-evident, it is not so obvious when considering white light control by dynamic phase (the operating principle

of SLMs) since the dynamic phase change through a medium is $2\pi n(\lambda)d / \lambda$, where $n(\lambda)$ is the refractive index, d the physical path length, and λ the wavelength. Clearly the phase change is inversely proportional to the wavelength. This is because the refractive index variation with wavelength in typical liquid crystals used in SLMs is small (about $5 - 10\%$) across a very wide spectral range spanning hundreds of nm [29]. Thus, the dynamic phase still provides a formidable constraint to control white light fields. This is a topical field, and recently it has been demonstrated in a manner that ensures the hologram is wavelength independent [29, 30]. Here we briefly outline the core idea to be used in a phase wrapped approach, based on Ref. [30], which we will use together with the propagation hologram to realise complete control of the white light field. Imagine that we wish to create our desired optical field in the first diffraction order, described by

$$u(x, y) = |u(x, y)| \exp\left(i\theta(x, y) + ik_x x\right), \tag{8}$$

where $u(x, y)$ is the field with phase $\theta(x, y)$ and k_x is a spatial carrier frequency as a consequence of a linear grating of pitch $p_x = 2\pi/k_x$. Here we assume the grating is applied in the x-axis but may be in any direction and the mathematics generalised to a tilt described by $\mathbf{k} \cdot \mathbf{r}$. Now if the hologram is calibrated for a design wavelength, λ_0 to produce a phase change of ϕ_0, then at a new operating wavelength λ the new phase change will be given by $\phi = \phi_0 \times (\lambda_0/\lambda)$. But SLMs do not allow for continuous phase profiles but rather modulated phase changes. Therefore, at the new operating wavelength the modulation is not over 2π but instead $2\pi \times (\lambda_0/\lambda)$. Consider now the phase-wrapped linear grating term: the pitch (or spatial carrier frequency) does not change, only the modulation depth. It is easy to show that such a wrapped saw-tooth phase ramp about the improper phase may be expressed as a suitably weighted superposition of plane waves, *i.e.*,

$$\exp\left(ik_x \frac{\lambda_0}{\lambda} x\right) \text{rect}\left(\frac{2}{p_x} x\right) \otimes \sum_{n=-\infty}^{\infty} \delta(x - np_x)$$
$$= \sum_{n=-\infty}^{\infty} \text{sinc}(\pi[n - (\lambda_0/\lambda)]) \exp\left(ink_x x\right). \tag{9}$$

Imprecise phase-wrapping results in several new diffraction orders appearing (denoted by n), but in multiples of the original carrier frequency, k_x. This seemingly innocuous fact has a significant consequence: since any complexed valued function can be written in the form of a linear phase gradient suitably sampled, *e.g.*, $|f(x_m)| \exp(i\phi_m) = |f(x_m)| \exp(i\phi_m x/x_m)\delta(x - x_m)$, this result implies that the new field at wavelength λ given by $\hat{u}_\lambda(x, y)$, differs from the desired field, $u(x, y)$, as

$$\hat{u}_\lambda(x, y) = \sum_{n=-\infty}^{\infty} \text{sinc}(\pi[n - (\lambda_0/\lambda)]) |u(x, y)| \exp\left(in\theta(x, y) + ink_x x\right). \tag{10}$$

If only the first order $n = 1$ is filtered out, then the hologram produces the field

$$\hat{u}_\lambda(x, y) = A_\lambda |u(x, y)| \exp\left(i\theta(x, y) + ik_x x\right) = A_\lambda u(x, y). \tag{11}$$

where $A_\lambda = \text{sinc}(\pi[\Delta\lambda/\lambda])$ is a constant amplitude term that only depends on the wavelength range used in the experiment. This is the only wavelength dependent term left in the equation and introduces an amplitude only modulation to the original field, *i.e.*, it is a slowly varying function with wavelength where over the entire visible range the efficiency changes by approximately 1%. Since this efficiency change is negligible, the approach can be considered as effectively controlling all spectral components of our white light field in an identical manner.

2.3. Virtual propagation

In addition to real space propagation, we also propagate our field using a motion-free approach that employs a SLM to mimic the angular spectrum method for beam propagation [31, 32]. Here we briefly summarise the idea. According to the angular spectrum approach an optical field can be regarded as a superposition of plane waves, which are spatial Fourier components, and travel in different directions. The propagation of our desired field $u(x, y, z = 0)$ in the direction of the z-axis can be described with the help of the transfer function of free-space $\exp(ik_z z)$:

$$u(x, y, z) = \mathcal{F}^{-1}\{\mathcal{F}[u(x, y, 0)]\exp(ik_z z)\}, \tag{12}$$

where $\mathcal{F}$ and $\mathcal{F}^{-1}$ denote the Fourier transform and its inverse, respectively, and k_z is the z-component of the wave vector. In a physical picture, the Fourier transformation can be realized by a lens, where the focal length f determines the wave vector components: $k_z = k\sqrt{1 - r^2/f^2}$. The phase function $\exp(ik_z z)$ can then instead of physically propagating the field also be implemented by digital means, *e.g.*, with an SLM. Since the phase pattern displayed on the SLM can be addressed dynamically, different propagation steps z can be programmed easily and the propagated beam can be recorded in a fixed observation plane. By way of example Fig. 1 shows step by step how different phase patterns affect the observation plane and how, as a last step, the virtual propagation scheme can be implemented.

3. Experimental concept and setup

Here we bring together the aforementioned tools to create and propagate a white light field, with the experimental concept sketched in Fig. 1. The Fourier transform of the optical field to be studied, $u(x, y, 0)$, is programmed by complex amplitude modulation onto the SLM to create the desired white light field. The SLM is then also programmed with the phase function $\exp(ik_z z)$ and the resulting field is (inverse) Fourier transformed by a lens to produce the propagated version of the optical field $u(x, y, z)$ for a propagation distance of z. The propagated output is finally recorded, using a CCD camera. This concept was implemented experimentally in the manner shown in Fig. 2, and used to demonstrate and compare the angular acceleration of a white light source for both real and digital propagation. We used a linearly-polarized, super-continuum laser (Fianium super-continuum SC400-4) which was expanded and collimated by a telescope ($f_1 = 15$ mm and $f_2 = 125$ mm) to illuminate the liquid-crystal display of a phase-only SLM (HoloEye, PLUTO-VIS, with 1920×1080 pixels of pitch 8 μm), labelled SLM$_1$. The hologram encoded on SLM$_1$ consists of two ring-slits, representing Durnin's ring-slit aperture [33, 34], which were programmed via complex amplitude modulation [35]. Each ring was encoded with a non-linear phase variation $\eta = \pi/5$ of order $\ell = +1$ and $m = -1$, respectively. This was achieved by multiplying the two ring-slits with the corresponding bracketed term in Eq. (4). Note, that the phase orders ℓ and m can be used to control the rotational symmetry of the beam [6]. The digital propagation was later performed by adding the phase $\exp(ik_z z)$ to the hologram on SLM$_1$, whereby we simultaneously create and virtually propagate the beam in the output plane. The Fourier transform of the field at the plane of SLM$_1$ was obtained with lens, L_3 ($f_3 = 200$ mm) and the resulting beam profile in the first diffraction order was selected by the pin-hole aperture (A). Due to the way the annular apertures are implemented on SLM$_1$, *i.e.*, by means of a blazed grating, the hologram is rendered wavelength independent in the first diffraction order (see section 2.2) [30]. For the first part of the experiment, whereby we investigated the real propagation of each individual wavelength (selected by an acousto-optic tunable filter within the source), a $10\times$ objective in conjunction with a CCD camera (PointGrey CCD) were positioned at plane A and moved along an optical rail to measure the rotation rates of the resulting petal structures. In the case of digital propagation the detection system remained static while the effect of propagation was digitally simulated on SLM$_1$ [31]. For the final part, where all wavelength components were
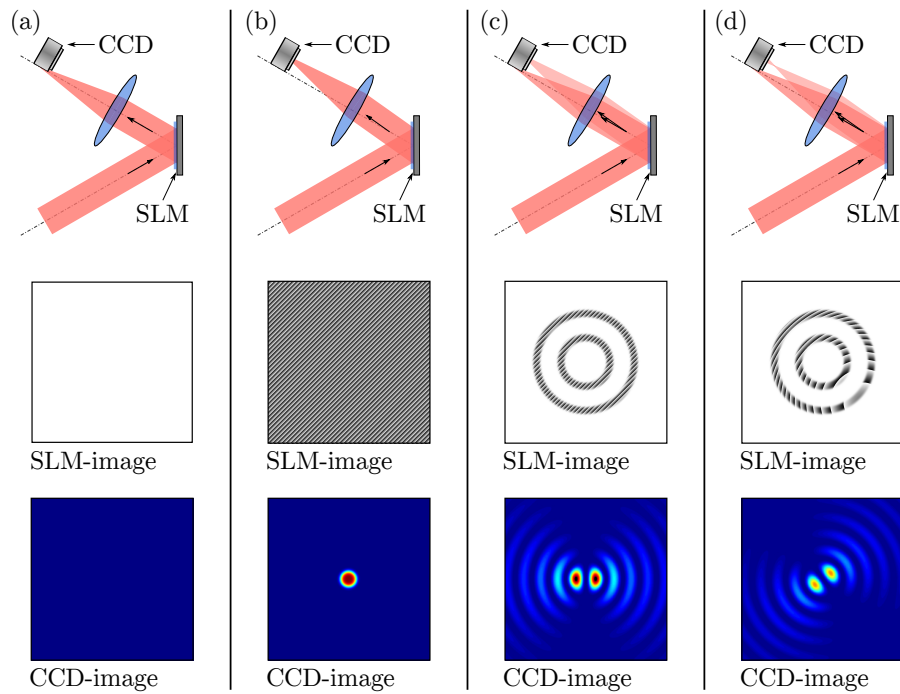
Fig. 1. The concept of the experiment requires the Fourier transform of the desired field $u(x, y, 0)$ to be encoded on the SLM in conjunction with a blazed grating. This procedure can be understood as follows: (a) With no grating present, all light remains on-axis and the CCD-image dark. (b) With a uniform grating, all light is redirected into the first diffraction order. (c) Local modulation of the grating enables amplitude modulation. In addition a slowly varying phase can be added to the grating whereby, for example, angular accelerating beams can be achieved. (d) When adding the phase given by the free-space transfer function $\exp(\mathrm{i}k_z z)$, the output plane is shifted with respect to z whereby the beam is digitally propagated without moving the CCD-camera.
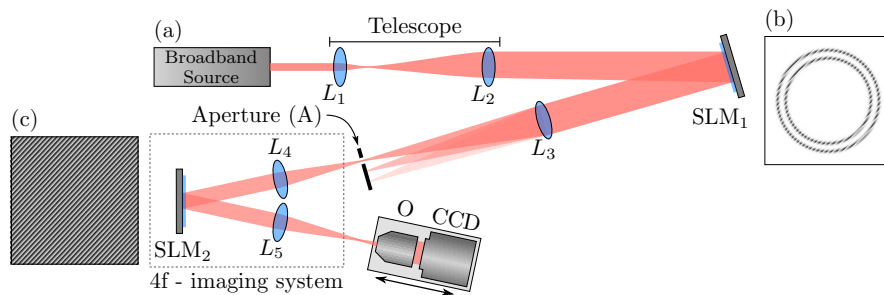

Fig. 2. Experimental implementation with (a) layout of our setup [L:Lens, SLM: Spatial Light Modulator, $f_1 = 15\,\mathrm{mm}$, $f_2 = 125\,\mathrm{mm}$, $f_3 = f_4 = 500\,\mathrm{mm}$, $f_5 = 200\,\mathrm{mm}$], (b) hologram on SLM_1 showing the amplitude-modulated annular apertures [$R_1 = 1.24\,\mathrm{mm}$, $R_2 = 1.56\,\mathrm{mm}$], (c) hologram on SLM_2 with inverted grating to SLM_1.

combined to obtain a full white light beam, the lens L_4, together with L_3, imaged SLM_1's filtered hologram on to the second SLM, SLM_2. To compensate for the angular dispersion caused by the blazed grating encoded on SLM_1, an identical (but inverted) blazed grating was encoded on SLM_2. The plane at SLM_2 was then Fourier transformed by the lens L_5 and the first diffraction order was imaged with a 10× objective onto our camera, allowing us to repeat the previously mentioned measurements on a multi-wavelength (white light) angular accelerating beam. Here a Logitech web camera was used in addition to the CCD camera as it allowed us to distinguish the individual wavelength components – this characteristic would not be noticeable on the PointGrey CCD.

4. Results and discussion

Using the introduced setup, first, a white light angular accelerating beam with a non-linear parameter $\eta = \pi/5$ was implemented. In order to assess the properties of each wavelength individually, the other wavelengths were disabled in an alternating fashion using the acousto-optic tunable filter implemented in the source. All available wavelengths in the range from 532 nm to 690 nm showed the behaviour expected from the monochromatic case [6], *i.e.*, a helical beam trajectory with an accelerating and decelerating rotation rate. Since the SLMs were calibrated to 632.8 nm, *i.e.*, a 2π phase-shift on the SLM equals 632.8 nm, this verifies that the wavelength-independent holographic implementation indeed works as anticipated. However, upon closer examination, it appears that the rotation period of the individual wavelengths is not strictly identical. By plotting the angular rotation of one of the lobes in the petal structure as a function of its propagation distance, as shown in Fig. 3(a), it is evident that the individual wavelength components would disperse during propagation. The reason for that lies in the fact that not only the phase profile but also the amplitude distribution influences the rotation period of the beam. In Eq. (5), this dependence is contained within Δk_z since

$$k_{z|n} = k(\lambda)\sqrt{1 - \frac{R_n^2}{f^2}}, \tag{13}$$

with $k(\lambda)$ being the wave number, R_n the radius of each ring on the SLM and f the focal length of the Fourier lens. Figure 3(b) shows a simulation based on Eq. (5) which matches our experimental result very well. Note that this, and all following theoretical graphs, are exclusively based on the analytical equations (5) to (7) and do not involve any fit-parameters.

Naturally, the dephasing of the spectral components will limit the propagation distance over which the beam can be considered a white light beam. Nonetheless, please notice that our experiment shows an exaggerated case where the wavelength range covers almost the entire visible spectrum. In typical applications, such as beam shaping with ultrashort laser pulses, this effect would be barely noticeable. In order to still account for the dephasing, multiple approaches are viable. For example, by cleverly engineering the chromatic aberrations of the system it could be possible to give each spectral component the appropriate ring radius, such that the dephasing is counteracted. Another option, which we want to follow here, is the digital propagation method. Since the propagation term $\exp(\mathrm{i}k_{z|n}z)$, in this case, is implemented alongside the beam on SLM_1, $k_{z|n}$ is rendered wavelength independent as well. Specifically, the wave number now follows $k = 2\pi/\lambda_c = $ const. with λ_c being the calibration wavelength of the SLM. Note, that this does not resolve the problem of dephasing in real space. However, in the observation plane, during digital propagation, all spectral components should remain in phase. This can be useful for applications where only a small volume is treated by the laser radiation, like for example laser trepanning of thin workpieces with femtosecond pulses, material surface studies, or optical delivery in microfluidic and optical trapping systems. Importantly, this compensation scheme is not a full compensation, but may be effective for applications where the dynamics at an individual plane are of primary interest.
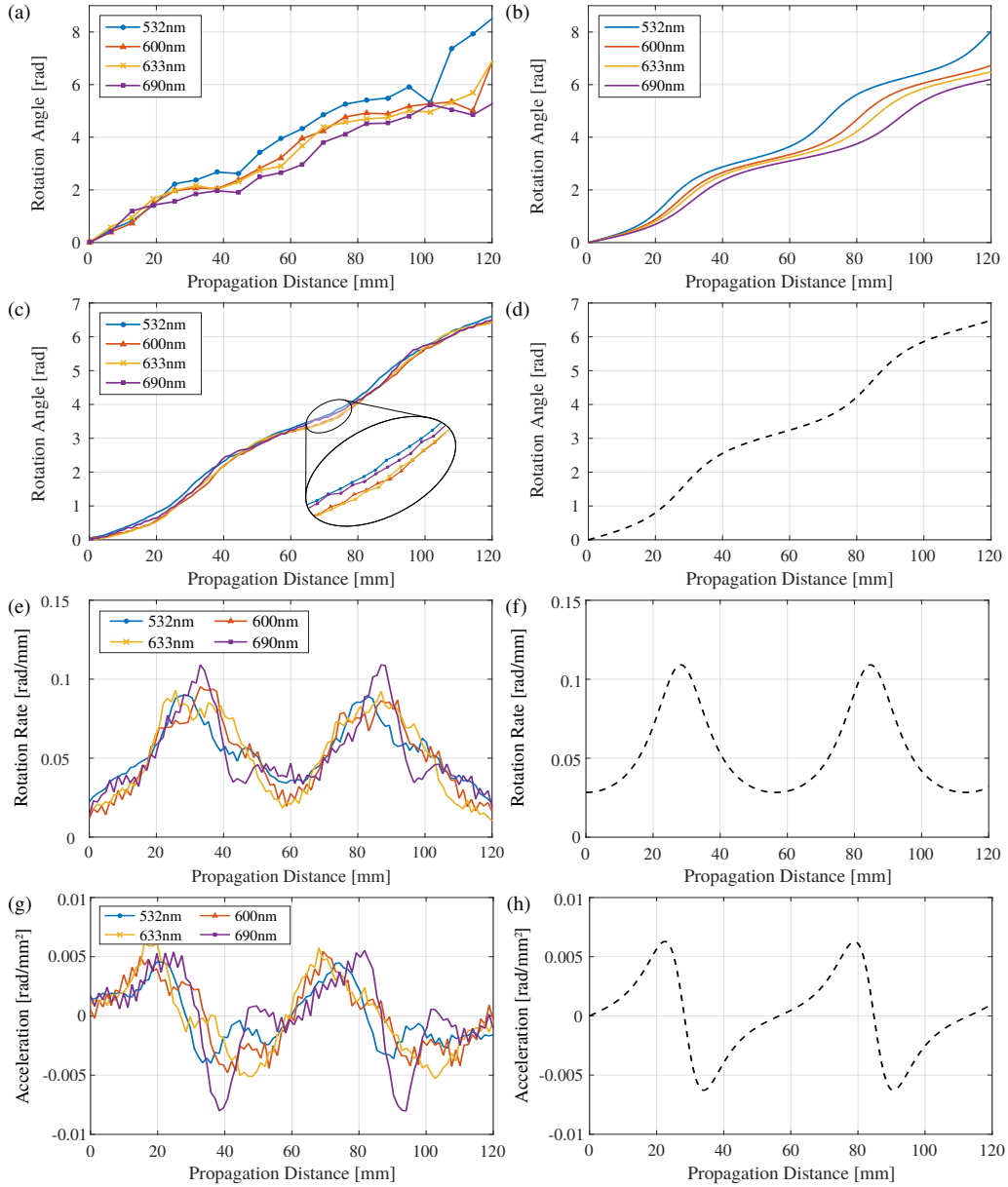
Fig. 3. Experimental results and simulations in real- and digital propagation for the spectral components of an angular accelerating white light beam with $\ell = +1$, $m = -1$ and $\eta = \pi/5$. Panels (a-b) show experiment (left) and simulation (right) of the rotation angle for real propagation. Panels (c-h) show experiment (left column) and simulations (right column) for digital propagation. Panels (e, g) are obtained from Panel (c) via numerical differentiation. Panels (d, f, h) are directly obtained from Eqs. (5) to (7) with $k = 2\pi/632.8$ nm.
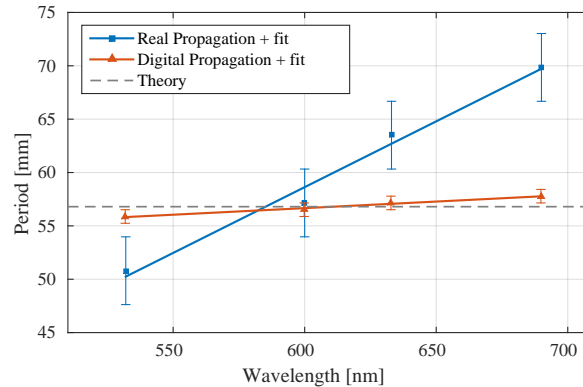
Fig. 4. Measured rotation period for real (blue) and digital (orange) propagation. Error bars refer to half the distance between two consecutive data points in Figs. 3 (a) and (c), respectively.

Figures 3(c)-3(h) show our experimental results as well as simulations for the digital propagation case. Both match each other extremely well, including the absolute numeric values. We also point out that comparison of Figs. 3(a) and 3(c) highlights the additional benefit of the virtual propagation tool: it resolves the propagation dynamics without unwanted perturbations due to experimental alignment errors: in (a) we note the "noisy" data due to small errors in alignment when moving the detector, whereas in (c) there are no moving parts and therefore the data is far "cleaner" and reveals the dynamics under study. In Fig. 4, we finally compare the obtained periods for real and digital propagation. As expected, the dephasing is reduced to almost zero within experimental uncertainty, though it is not removed entirely. This small discrepancy could be based on the pixel-based and digitalized nature of the SLM. The theoretical concept we employed here [30] is after all based on continuous filters and does not include those specific technological limitations of the SLM. Nevertheless, a small dephasing is not a major obstacle as it is hardly noticeable over the anyway (physically) limited propagation range of angular accelerating beams.

For our last experiment, all wavelength components were adjusted in brightness to contribute equally to the CCD or webcam image, respectively, and were spatially combined using SLM_2. Moreover, the nonlinear parameter was adjusted to $\eta = \pi/3$ to create an even more obvious angular acceleration with a period of approximately 14 mm. Figure 5 provides an iso-intensity graph of the subsequently recorded volume data where the iso-surface corresponds to two-thirds of the peak intensity. In addition, a short movie recorded with the aforementioned webcam can be found in the supplementary material to this article (see Visualization 1).

5. Conclusion

In this work we have studied the propagation dynamics of angular accelerating white light beams where such beams have been created and propagated using a phase-only SLM. The approach allows for virtual and real propagation to be studied simultaneously, and may be generalised to any structured white light beam. We have compared both the digital and real propagation and found that while in real propagation dephasing occurs, the digital propagation becomes non-dispersive due to the wavelength-independence of the employed holograms. We expect this work to inspire further studies in the application of structured white light, for example, in controlling white light, supercontinuum sources and ultrafast lasers for spectroscopy, microscopy, machining and lab-on-chip applications.
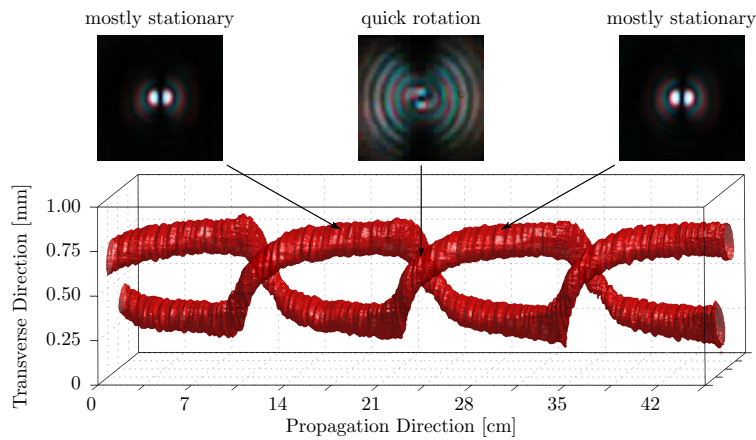
Fig. 5. Recorded behaviour for a white light angular accelerating beam with $\ell = +1$ and -1, and $\eta = \pi/3$. Top: Beam profiles recorded with a commercial rgb-webcam. Bottom: Iso-intensity plot obtained from beam profiles recorded with a high-quality monochromatic CCD. The iso-surface corresponds to two-thirds of the peak intensity. All wavelength components were set to contribute equally to the overall exposure.

Funding